Atmospheric Research 280 (2022) 106461

Contents lists available at ScienceDirect

Atmospheric Research

journal homepage: www.elsevier.com/locate/atmosres

Skill assessment of Saudi-KAU and C3S models in prediction of spring season rainfall over the Arabian Peninsula

Mansour Almazroui [a,b,*], Salman Khalid [a], Shahzad Kamil [a,c], Muhammad Ismail [a], M. Nazrul Islam [a], Sajjad Saeed [a,d,e], Muhammad Adnan Abid [d], Muhammad Azhar Ehsan [f], Ahmed S. Hantoush [a]

[a] Center of Excellence for Climate Change Research/Department of Meteorology, King Abdulaziz University, PO Box 80208, Jeddah 21589, Saudi Arabia
[b] Climatic Research Unit, School of Environmental Sciences, University of East Anglia, Norwich, UK
[c] Climate Change Impact and Integration Cell (CIIC), Pakistan Meteorological Department, Islamabad, Pakistan
[d] The Abdus Salam International Center for Theoretical Physics, Trieste, Italy
[e] Department of Earth and Environmental Sciences, KU Leuven, Leuven, Belgium
[f] International Research Institute for Climate and Society, Columbia Climate School, Columbia University, Palisades, NY, USA

ARTICLE INFO

Keywords:
Arabian Peninsula
Coupled global climate models
Potential predictability
Prediction skill

ABSTRACT

A skillful prediction of precipitation has great value, particularly for regions that suffer from water stress. In this study, we assess the potential predictability and skill of the Copernicus Climate Change Service (C3S) and Saudi-KAU models in their simulation of precipitation over the Arabian Peninsula during spring (March–May) for the period 1993–2016. For this purpose, data from individual models as well as the multi-model ensemble (MME) is used. The prediction data for MAM precipitation initialized at Feb (Lead 1), Jan (Lead 2), and Dec (Lead 3), were obtained from the 5 C3S and Saudi-KAU coupled global climate model. The potential predictability was computed by evaluating the signal to noise ratio and the theoretical limit of correlation skill, while the prediction skill was estimated from the temporal anomaly correlation co-efficient. The results show that the Saudi-KAU, CMCC, and UKMO models have slightly higher potential predictability of about 0.25, 0.35, and 0.25 respectively, as compared to other models. It is also observed that individual models as well as their MME show a high (low) potential predictability over southwestern (northern) regions of the Peninsula. Moreover, the Saudi-KAU, CMCC, and MME show a reasonably good correlation skill (0.68, 0.59, and 0.57) while the SEAS model displays lower skill (0.14) for spring precipitation. All model simulations reveal a decrease in prediction skill for longer lead times. On the other hand, the individual models and their MME successfully reproduced the Pacific (i.e. ENSO) teleconnection patterns while displaying lower skill over the tropical Atlantic Ocean. The results indicate that the model biases have negative impacts on potential predictability and prediction skill over the Arabian Peninsula during the spring season.

1. Introduction

Precipitation is a key variable of the hydrological cycle, and its timely prediction is very important for the better management of regional water resources, agriculture, and related services. The climate of the Arabian Peninsula is arid to semi-arid in nature, and generally associated with high temperature and low precipitation (Almazroui et al., 2012). The climate of the Arabian Peninsula is strongly influenced by the South-Asian Monsoon and by Mediterranean synoptic scale systems (Almazroui et al., 2017). The South-Asian Monsoon impacts the southwestern region while the northern region remains under the influence of eastward propagating synoptic scale Mediterranean systems (Kamil et al., 2017). Moreover, the complex topography of the region plays an important role in characterizing its climatic conditions. The topography of the Arabian Peninsula consists of highlands along the western and southwestern boundaries, and three big deserts, namely Nafud (north), Al-Dahna (interior) and the largest continuous sand desert Rub Al-Khali (southeast). Furthermore, the Peninsula is

* Corresponding author at: Center of Excellence for Climate Change Research, Department of Meteorology, King Abdulaziz University, PO Box 80208, Jeddah 21589, Saudi Arabia.
E-mail address: mansour@kau.edu.sa (M. Almazroui).

https://doi.org/10.1016/j.atmosres.2022.106461
Received 22 June 2022; Received in revised form 2 September 2022; Accepted 1 October 2022
Available online 8 October 2022

surrounded by water bodies on three sides; the Red Sea (west) Arabian Gulf (east) and the Indian Ocean (south) are major sources of moisture transport (Patlakas et al., 2021; Almazroui, 2020). Common weather phenomena associated with the region include drought, heatwaves, and dust storms, along with temperature and precipitation extreme events (Alamgir et al., 2019). On the other hand, the IPCC (2022) AR6 report and numerous other studies (e.g., Kotwicki and Al Sulaimani, 2009; Almazroui, 2013; AlSarmi and Washington, 2014; Barfus and Bernhofer, 2014; Pal and Eltahir, 2016; Bucchignani et al., 2018; Attada et al., 2019; Syed et al., 2019; Almazroui and Saeed, 2020; Almazroui et al., 2020; Odnoletkova and Patzek, 2021; Chaturvedi et al., 2022) highlighted that the Arabian Peninsula is vulnerable to climate change. To avoid the consequences of climate change such as socio-economic losses at local and regional scales, and to avoid catastrophes, seasonal predictions can play a vital role in assisting policymakers to take necessary actions in a timely way (Wang et al., 2015). In recent decades, the numerical weather predication skills of the models have significantly improved, due to better representation of various features associated with the dynamical models. The latest generation of dynamical models accurately describe the different components of the climate system and their interactions. Recent studies indicate that model uncertainty can be reduced by improving the initial conditions, model physics, and by increasing the ensemble size (Barnston et al., 2012; Ehsan et al., 2017).

Numerous studies have addressed the seasonal prediction of temperature and precipitation over various regions of the globe using different coupled climate models. Khan et al. (2017) examined the global seasonal precipitation forecasts by using the improved sea surface temperature predictions for the period 1981 to 2008. Similarly, Jia et al. (2015) improved the seasonal prediction of temperature and precipitation over land in a high resolution GFDL climate model. In another study, Weisheimer and Palmer (2014) discussed the reliability of seasonal climate forecast for the period 1984 to 2014, by using the ECMWF SYS4 climate models. Correspondingly, Barnston et al. (2019) assessed the NMME models prediction skill for El Nino Southern Oscillation (ENSO) during the period 1982 to 2015. Using the 7-NMME models datasets, the seasonal predictability and prediction skill of global temperature and precipitation was studied by Becker and den Dool (2014). Krakauer (2019) analyzed the global temperature trends and prediction skill of NMME models during the period 1982 to 2015. Osman and Vera (2017) investigated the climate predictability and prediction skill over South America by using the CHFP models. Wei et al. (2013) examined the seasonal predictability of summer precipitation over the Huaihe river basin in China by using the APCC models for the period 1981 to 2003. Likewise, Rana et al. (2018) examined the seasonal prediction of winter precipitation anomalies over central southwest Asia. The potential predictability and forecast skill of sea surface temperature over the tropical Indian Ocean and eastern central Pacific was investigated by Jin et al. (2018) for the period 1960 to 2005. Cheng et al. (2011) evaluated the relationship between the predictability and forecast skill of ENSO on various time scales. In addition, Cash et al. (2019) explored the NMME models biases and forecast skill over South Asia during the period 1982 to 2010. The investigation revealed that the construction of multi-model ensemble mean (MMEM) by small number of ensemble members outperform compared to MMEM constructed with large number of ensemble members. Furthermore, the Nobakht et al. (2021) assessed the precipitation skill using C3S models over the Iran. Their findings shows that ECMWF and UKMO models skillfully simulate the precipitation and the Meteo-France has low skill at Iran. Giuntoli et al. (2022) examined the predictability of Mediterranean weather regimes for period 1993 to 2016. The results of this study shows that the C3S models well reproduce ENSO teleconnections and the predictability in Mediterranean region during the intense ENSO years. Moreover, the performance of C3S models for mean and extreme precipitation over Africa is evaluated by Gebrechorkos et al. (2022). It is revealed in the investigation that models show moderate skill for drought and weak skill for heavy to very heavy precipitation days. However, the ECMWF and UKMO have high skill compared to the other models. Similarly, several studies delineate the potential predictability and prediction skill of temperature and precipitation over the Arabian Peninsula by using various dynamical models for different seasons (i.e. Abid et al., 2016; Ehsan et al., 2017; Ehsan et al., 2019).

The Saudi-KAU GCM developed by the Center of Excellence for Climate Change Research (CECCR), King Abdulaziz University, Jeddah, Saudi Arabia, facilitates various options for seasonal climate simulations. These options include two dynamical cores (Spectral and Finite Volume), three different Ocean components (MOM2.2, Nemo3.6, and MOM5.1), and different physical schemes (e.g., Radiation, Convection, Planetary boundary layer, Land, Microphysics, and Sand/Dust) that numerically simulate different components of the climate system and their interactions (Almazroui et al., 2017). The model is capable of generating seasonal to sub-seasonal forecasts along with long-term climate simulations. So far, the seasonal prediction skills of this model have not been explored in much detail. Some very limited studies analyzed the performance of this model in the simulation of seasonal and sub-scale climate over different parts of the globe (i.e. Ehsan et al., 2017a, b; Abid et al., 2018; Rahman et al., 2018; Almazroui et al., 2022; Rashid et al., 2022). On the other hand, the C3S system consists of various models that belongs to different European countries. The seasonal framework is based on five well-known forecast systems such as European Centre for Medium Range Weather Forecasts (ECMWF), Météo-France (METEOF), UK Met Office (UKMO), Deutscher-Wetterdienst (DWD), and Centro Euro-Mediterraneo sui Cambiamenti-Climatici (CMCC) (Vitart et al., 2017; Vitart and Robertson, 2018). Some studies have investigated the potential predictability and skill of C3S models over various regions during different seasons (e.g., Bett et al., 2019; Manzanas et al., 2014; Contreras et al., 2020; Min et al., 2020; Giuntoli et al., 2021; Risbey et al., 2021). To date, no study has comprehensively evaluated the precipitation prediction skills of the Saudi-KAU and C3S models over the Arabian Peninsula.

In the present study, we examined the potential predictability and prediction skill of spring precipitation over the Arabian Peninsula with the C3S and Saudi-KAU models. The main reason to focus on spring is its dominant contribution to the total annual rainfall. Alsaaran and Alghamdi (2021) revealed that winter and spring are the wetter seasons and that spring contributed around 40% to the total annual rainfall of the Arabian Peninsula. In addition, Nelli et al. (2021) showed that extreme precipitation events are common in spring over the Peninsula, particularly over southern regions due to low level convergence and moisture advection through the Arabian Sea/Gulf and the Red Sea. Further, Patlakas et al. (2021) showed that passage of the desert front and thermal low from Sudan was primarily responsible for triggering the convective activity and bringing intense rainfall over the northern Red Sea and central Saudi Arabian regions during spring. Hence the main objective of the present study is to evaluate the potential predictability and prediction skill of spring precipitation over the Arabian Peninsula by utilizing the Saudi-KAU and C3S CGCMs. The next section describes the data and methods.

2. Data and methods

2.1. Observational data set

In this study, we used the "Global Precipitation Climatology Project (GPCP)" monthly mean data set with horizontal grid resolution 2.5° × 2.5°. The GPCP data is based on various satellite data sets over ocean and land, rain gauges on land, and a sounding dataset. This combination of datasets provides a complete rainfall analysis over both land and ocean (Adler et al., 2003). However, the sea surface temperature of the Extended Reconstructed Sea Surface Temperature (ERSST) with a spatial resolution of 2° × 2° was also acquired for various analysis (Huang et al., 2017).

2.2. Model simulations

The Copernicus Climate Change Service (C3S) models and Saudi-KAU GCM simulations were used in the present study. The C3S state of the art models such as ECMWF SEAS5 (Johnson et al., 2019), Meteo-France-System7 (Guérémy et al., 2021), UK Met-office GlosSea5 (MacLachlan et al., 2015), DWD GCF2.0 (Fröhlich et al., 2021), and CMCC (Sanna et al., 2017) generated the seasonal predictions. Additionally, the Saudi-KAU GCM (Almazroui et al., 2017) seasonal prediction data was also incorporated in the investigation. The Saudi-KAU GCM is operational at the Center of Excellence for Climate Change Research and produces seasonal and sub-seasonal forecasts.

2.3. Experimental setup of Saudi-KAU GCM

The spectral dynamical core of the Saudi-KAU GCM is based on the Bourke (1974) numerical structure. The model solves the prognostic equations of divergence and vorticity and diagnostically derived the horizontal and vertical components of wind. Linear calculations are performed in spectral/wave-space by applying the Fast Fourier and Legendre transforms at each time step, whereas the non-linear calculations are done in grid space. A semi-implicit time integration scheme is utilized in the upgraded model version. Model initialization is based on atmosphere and ocean nudging at each time step. The temperature, surface pressure, specific humidity, and u, v components of wind are nudged in the Atmospheric Global Climate Model (AGCM) while the salinity and potential-temperature are nudged in Ocean Global Climate Model (OGCM). The Saudi-KAU AGCM is able to perform simulations at various horizontal and vertical resolutions. In the present work we utilized the spectral T42 horizontal resolution (2.8°x2.8°) and 20 vertical levels. Initial conditions at 6 hourly frequencies are available for the period 1 Mar 1993–31 Dec 2016. For the generation of ensemble members, the lagged-averaged forecast perturbation method was used (Hoffman and Kalnay, 1983). For atmospheric initial conditions, the perturbation interval is 6-hourly whilst the ocean initial conditions remain consistent for all ensembles. The Saudi-KAU CGCM forecast data set consists of 20 ensemble members, each starting on the first of every month and extending out to 12 months beyond the start date.

We targeted the spring season (Mar-May) and used the hindcast data of Lead 1–3 (Feb-Dec) for the period 1993–2016. The C3S models run at spatial resolution $1^\circ \times 1^\circ$ while the Saudi-KAU GCM was regridded to the same horizontal resolution for homogeneity. Further details of the prediction data are given in Table 1.

2.4. Method

We assessed the potential predictability and prediction skill of the above models for spring precipitation over the Arabian Peninsula for 1–3 month lead times (i.e. for jobs starting Feb-Dec). It was found that the multi-model ensemble mean (MME) provides a higher level of confidence than a single model instance (Watson et al., 2001; Tebaldi and Knutti, 2007; Pincus et al., 2008), therefore, we also analyzed the MME. For model validation, we employed different statistical methods (e.g., mean, bias, root mean square error (RMSE), standard deviation, correlation) (Ehsan et al., 2017). Similarly, the precipitation variability patterns provided by the ensemble mean, by each ensemble member, and by observations, all provide measures of the actual and potential skill. Grid box analysis is performed to examine the temporal anomaly correlation between predicted and observed data sets for various lead times. The best models are considered to be those that have low bias, small RMSE, and high correlation values, along with similar variance patterns relative to the observations. Likewise, the persistent prediction skill is also assessed to examine the skill of models and MME at different Lead Time (0–3) for 12 running season. For this, we evaluated the persistent skill of observation by using lag k = 1 autocorrelation and construct baseline to verify the prediction skill of the models at various lead times. The skill is considered valuable when prediction skill is surpasses this baseline, otherwise the skill is useless (Zuo et al., 2016). The potential predictability of spring precipitation over the Arabian Peninsula is evaluated from the inter-annual variability of an ensemble mean, and the variability of individual ensemble members relative to their mean, known respectively as the signal and noise variance. Signal and noise variance are expressed as follow (Rowell et al., 1995; Rowell, 1998).

$$Signal = \frac{1}{N-1}\sum_{k=1}^{N}(\overline{P_k} - \overline{P})^2$$

$$Noise = \frac{1}{N(n-1)}\sum_{k=1}^{N}\sum_{m=1}^{n}(P_{km} - \overline{P_k})^2$$

Here P is the precipitation, k denotes individual years, and m indicates ensemble members. $\overline{P_k}$ is an ensemble mean in year k, while $\overline{P}$ is the long-term climatology of the ensemble mean. The signal to noise variance ratio (S/N) defines the potential predictability (Kang and Shukla, 2006). Similarly, the Rlimit/Theoretical limit is evaluated to interpret the predictability. The value of Rlimit is between 0 and 1; a value of 0 (zero) means "no predictability" while a value of 1 (one) represents "perfect predictability"(Bahaga et al., 2015).

$$R_{limit} = \sqrt{\frac{SI}{SI+N}}$$

where SI represents signal variance and N is the noise. Then, SI + N is the total variance. The computation of teleconnection patterns provides a further measure of the skill of an individual model and the MME. Generally, the skillful models are deemed to be those that are able to reproduce the teleconnection patterns obtained from observations.

Table 1
The C3S models and Saudi-KAU GCM hindcast configuration.

Sr. no	Models	Acronym of models	Ensembles members	Atmospheric component	Ocean component	Sea-ice component
1	ECMWF SEAS5 System 5	SEAS5	25	IFS (TCo319, equiv. to N320: ~ 36 km, 91 levels IFS: TCo319, equi. to N320: 36 km, L91	NEMO: 0.25°, L75	LIM
2	METEO FRANCE System 7	METEOF	25	ARPEGE-Climat: Tl359, 0.5°, L91	NEMO 3.6: 0.25°, L75	Gelato
3	UKMO GloSea6-GC2	UKMO	28	UM: N216, 60 km, L85	NEMO: 0.25°, L75	CICE
4	DWD GCFS2p1	DWD	30	ECHAM6: T127, 100 km, L95	MPIOM: 0.4°, L40, Sea-ice included	–
5	CMCC SPSv3p5	CMCC	40	CSEM: 1°, 100 km, L46	NEMO: 0.25°, L50	CICE
6	Saudi-KAU GCM test_kau_4.3	KAU	20	KAU_4.3: T42, 2.8°, L20	MOM2.2: 1°, L32	–

3. Results and discussion

3.1. Observed and simulated precipitation climatology

The spatial distribution of spring precipitation climatology from observations, C3S and Saudi-KAU GCMs is shown in Fig. 1. The observed precipitation climatology shows the highest amount of precipitation (~32 mm/month) over the southwestern quadrant, and the lowest rainfall (~4–8 mm/month) over the northwestern and southeastern regions of the Peninsula (Fig. 1a). Moreover, the SEAS model climatology is almost in line with the observations. The high (low) precipitation ~32 (< 4) mm/month is found at the southwestern (northwestern and southeastern) regions of the Peninsula (Fig. 1b). Similarly, the METEOF precipitation climatology shows maximum rainfall (> 32 mm/month) over the southwestern region while the minimum precipitation (~4–8 mm/month) fell over the northwestern and southeastern regions (Fig. 1c). Further, the UKMO model successfully captured the mean precipitation pattern relative to observations (Fig. 1d). Nevertheless, the spring climatology of DWD exhibits slightly high precipitation (~12 mm/month) over the southwestern coastal regions while the precipitation remains under 4 mm/month over the other domains of the Peninsula (Fig. 1e). The CMCC spring climatology is shown in Fig. 1f, where it can be observed that the model performance is reasonably good over the southern regions, but somewhat too low over central and northern regions relative to observations. On the other hand, the spring climatology of the Saudi-KAU model displays relatively high precipitation (~24 mm/month) over the southwestern quadrant, and relatively low amounts (~8 mm/month) over the southeastern regions (Fig. 1g). The MME spring mean pattern is similar to observations, with high (low) precipitation over the southwestern (northwestern and southeastern) regions (Fig. 1h).

Following Almazroui and Saeed (2020), we also examined the contribution of spring precipitation to total annual rainfall over the Arabian Peninsula. The spatial distribution of the spring precipitation

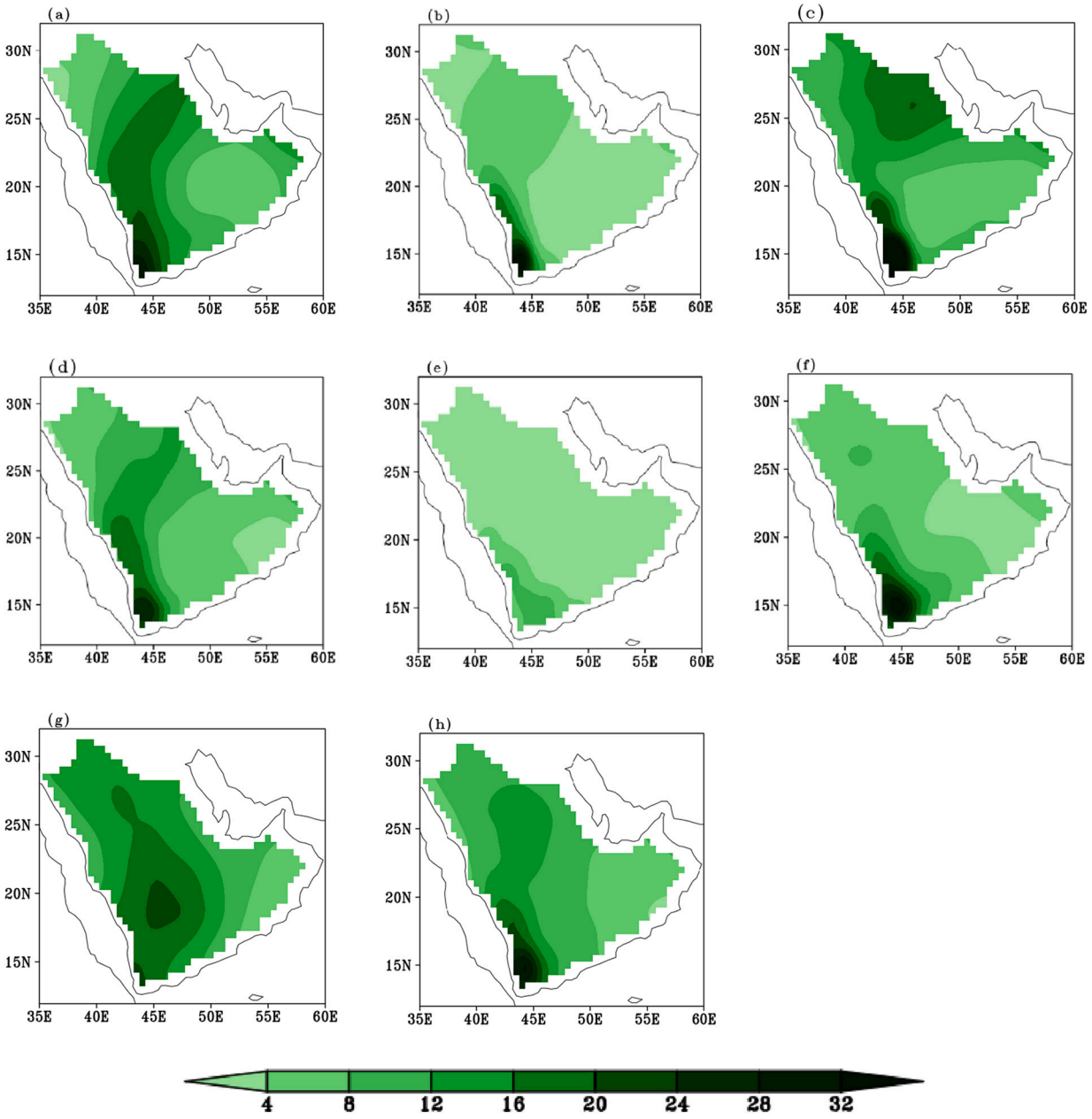

Fig. 1. Observed and simulated precipitation (mm/month) climatology during the spring season, from (a) GPCP, (b) SEAS, (c) METEOF, (d) UKMO, (e) DWD, (f) CMCC, (g) Saudi-KAU CGCM, and (h) MME for the period 1993–2016.

contribution to the annual total over the Peninsula is shown in Fig. 2a. Spring contributed the largest fraction of precipitation (~ 50%) over the central and some southern regions, and the smallest fraction (~ 30%) over the northern region. During spring, the northern and central regions remain under the influence of the North African low, which brings rainfall and thunderstorms. However, the southern regions receive rainfall due mainly to convective systems that develop as a result of land-sea temperature contrast and the orographic uplift mechanism (Hasanean and Almazroui, 2015; Dasari et al., 2018). For spring precipitation variability, the empirical orthogonal function (EOF) was evaluated and is presented in Fig. 2b. The first model depicts spring precipitation variance of ~58% for the entire selected domain. The maximum variance is found over the central and southwestern regions while the minimum variance is occurred over the northwestern quadrant. Furthermore, the time series analysis of Arabian Peninsula spring precipitation index, PC1 and Nino 3.4 index are shown in Fig. 2c. The result shows that coherence pattern of precipitation index and PC1 whereas the Nino 3.4 is also in line. The correlation co-efficient value

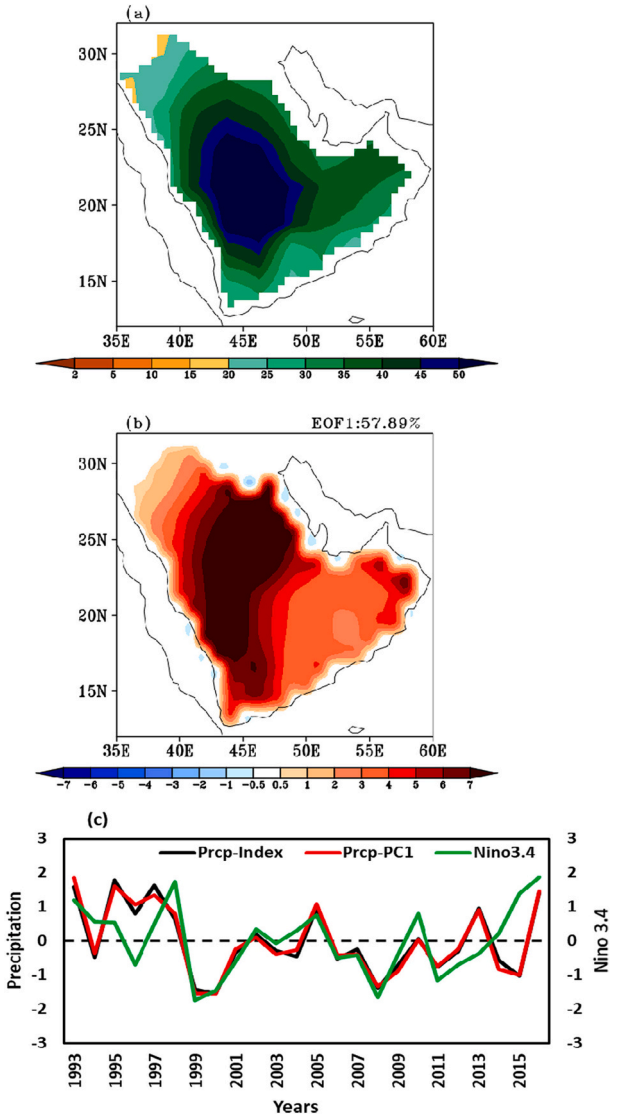

Fig. 2. (a) Spring season precipitation contribution (%) to the total annual precipitation (b) precipitation variability, as obtained from the leading EOF mode (EOF1) and the leading EOF mode shows variance about 57.89%, (c) Precipitation variability of PC1, AP-Index and Nino 3.4 during the period 1993 to 2016. The correlation co-efficient value between AP-Index and PC1 is 0.98 while the correlation values of Nino3.4 and AP-Index (PC1) are 0.62 (0.61).

(~0.98) between Arabian Peninsula precipitation index and PC1 while the Nino 3.4 and Arabian Peninsula precipitation index (PC1) is around 0.61 (0.62). This shows that ENSO significantly modulates the Arabian Peninsula spring precipitation. During warm phase (El-Nino) the precipitation amplify over the region and in cold phase (La-Nina) it suppressed. These results are consistent with the previous investigation on ENSO relationship with Arabian Peninsula precipitation (Kang et al., 2015; Sandeep and Ajayamohan, 2018).

The spring precipitation bias patterns of the C3S and Saudi-KAU GCMs relative to observations are presented in Fig. S1. The SEAS5 model precipitation bias pattern shows that the model underestimated precipitation (~16 mm/month) throughout the Peninsula except over sparse regions of the southwestern coastal belt where the model overestimated precipitation by up to 12 mm/month (Fig. S1a). The METEOF model overestimated precipitation (~8 mm/month) over the northern, eastern, and southwestern regions while the model underestimated precipitation (12 mm/month) over the western region (Fig. S1b). Consequently, the UKMO, DWD, and CMCC bias patterns are consistent. It is clear that the models underestimated the precipitation over almost all the Peninsula. A large (small) negative bias appears over the central (northwestern and southeastern) region of the Arabian Peninsula (Fig. S1c-e). Furthermore, the Saudi-KAU overestimated the precipitation within a range of 4–16 mm/month over the entire Peninsula (Fig. S1f). However, the MME shows a negative bias (~ 8 mm/month) over the central and some southern regions, and a positive bias over the northern region (Fig. S1g). Overall, all the models and MME show smaller biases over the northwestern and southeastern regions, but larger biases over central and western coastal regions.

3.2. Spatial patterns of root mean square error and standard deviation

The spatial distribution of the RMSE of individual models and the MME is presented in Fig. 3. The SEAS5 model RMSE pattern shows a high value (~ 24 mm/month) over the central and western regions, and low values over the northwestern and southeastern quadrants (Fig. 3a). Similarly, the METEOF pattern displays high (low) values of ~28 (4–8) mm/month over the southwestern (northwestern and southeastern) regions (Fig. 3b). The UKMO, DWD, and CMCC models all depict almost identical RMSE patterns. The high (low) values are occurred over the western and central (northwestern, southeastern) regions (Fig. 3c-e). The Saudi-KAU simulated maximum RMSE (~24 mm/month) over the southwestern region, and minimum values (< 8 mm/month) over the southeastern quadrant (Fig. 3f). Meanwhile, the MME has high (low) RMSEs of ~16 (< 6) mm/month over the southwestern and central (northwestern and southeastern) regions (Fig. 3g).

Fig. 4 shows the observed and simulated distribution of the standard deviation (SD) of precipitation over the Arabian Peninsula. The spatial pattern of observed SD shows high variability (8–12 mm/month) over the central and western regions, while low variability occurred over the northwestern and southeastern regions. The similar pattern of SD is obtained from SEAS5 model while METEOF model shows slightly high variability relative to observations. The UKMO model shows slightly high variability over the southwestern and central regions and low variability over northern and southeastern regions. The DWD pattern of precipitation SD displays high (low) variability over the southwestern (northern) regions. Meanwhile, the SD patterns of the CMCC and Saudi-KAU models, and the MME, have a great resemblance to each other.

3.3. Assessment of precipitation prediction skills

Fig. 5 presents the spring precipitation correlation skill of the C3S and Saudi-KAU models and the MME with respect to the observations. The SEAS5 model exhibits weak positive (negative) correlation over sparse northern (southeastern) regions (Fig. 5a). The METEOF model shows a positive correlation (~ 0.2) over western, central, and southern coastal regions, whereas the model skill is poor over northern and

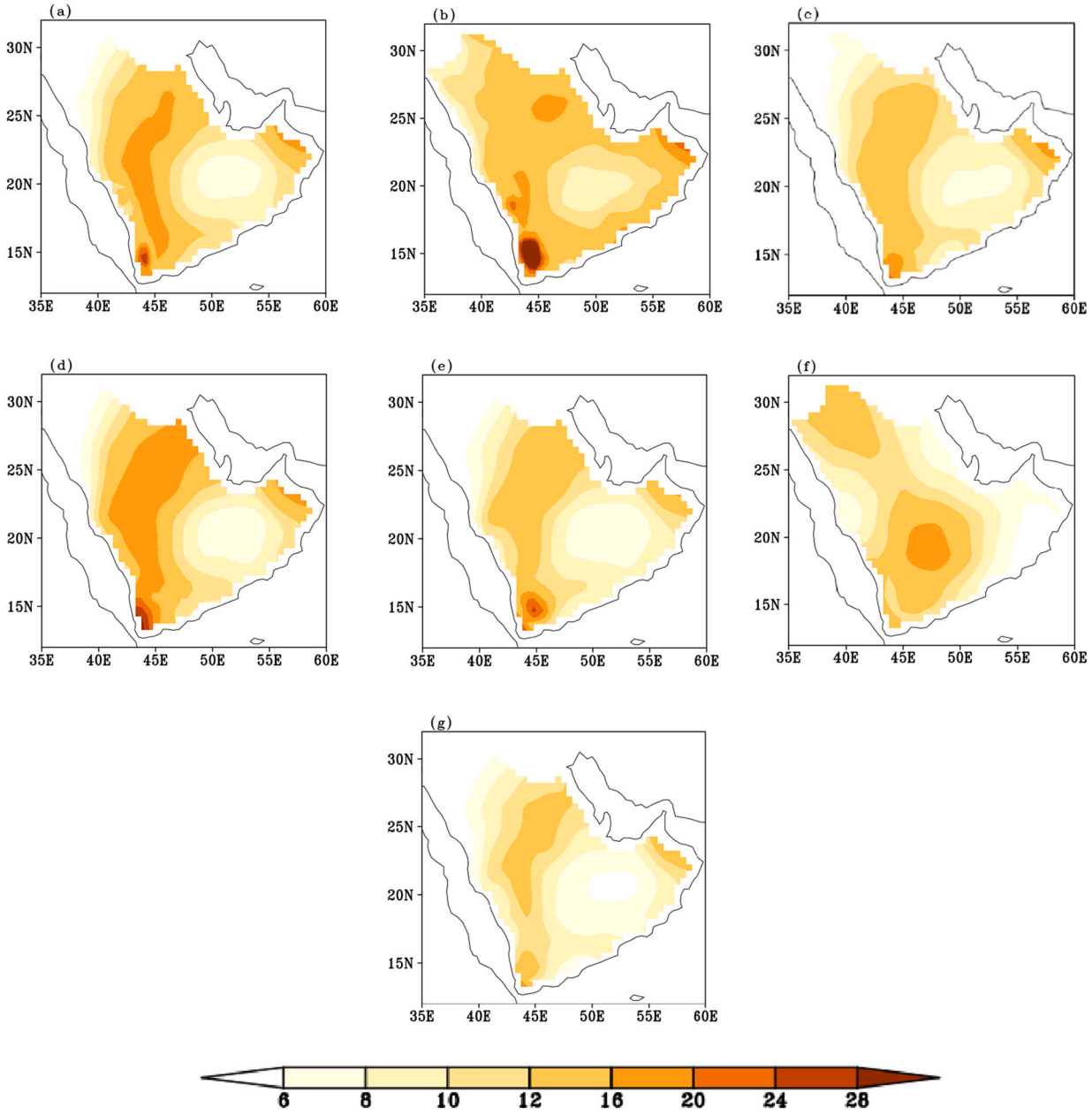

Fig. 3. Simulated Root Mean Square Error (RMSE) during the spring season, from (a) SEAS, (b) METEOF, (c) UKMO, (d) DWD, (e) CMCC, (f) Saudi-KAU CGCMs, (g) MME for the period 1993–2016.

eastern regions (Fig. 5b). The UKMO correlation skill pattern demonstrates positive correlation (~0.2) over the northeastern and southwestern quadrants whereas weak skill is observed over the northwestern and southeastern regions (Fig. 5c). The DWD model has positive correlation over southern regions but a weaker relationship elsewhere (Fig. 5d). The CMCC and Saudi-KAU models and the MME display slightly higher skill compared to other models over almost all the Peninsula. In particular, CMCC and the MME show relatively high skill (~0.4) over the northeastern and southwestern quadrants, but lower coefficient values (< 0.4) over the other regions. The Saudi-KAU model depicts relatively high skill over the southeastern region (Fig. 5e-g). Fig. 6 displays a Taylor diagram (Taylor, 2001) showing correlations and standard deviations of spring rainfall from the C3S and Saudi-KAU models and the MME with observations. In Fig. 6, the CMCC and Saudi-KAU models and the MME show relatively high correlations (≥ 0.6), while the CMCC and Saudi-KAU models also display standard deviation values that are closer to observations. Meanwhile, the SEAS5, METEOF, UKMO, and DWD models all have correlation co-efficient values <0.4 along with low standard deviations relative to observations. The grid box analysis in Fig. 7 shows the temporal anomaly correlation co-efficient of the C3S and Saudi-KAU models and the MME with observations, for different Lead times (1–3). The CMCC and Saudi-KAU models and the MME show significantly higher correlations for Lead 1 and Lead 2 compared to other models. However, all the models report low correlations for Lead 3. The SEAS5 and DWD models show low skill over the Arabian Peninsula for all Lead times.

3.4. *Relative operating characteristic (ROC)*

We further performed relative operating characteristic (ROC) analysis to examine the probability forecast based on hit rate and false-alarm rate (Fig. 8). The ROC diagram describes the probability forecast skill of models for events with likelihood below normal, normal, and above normal. The ROC curve bending toward the hit rate axes indicates a high

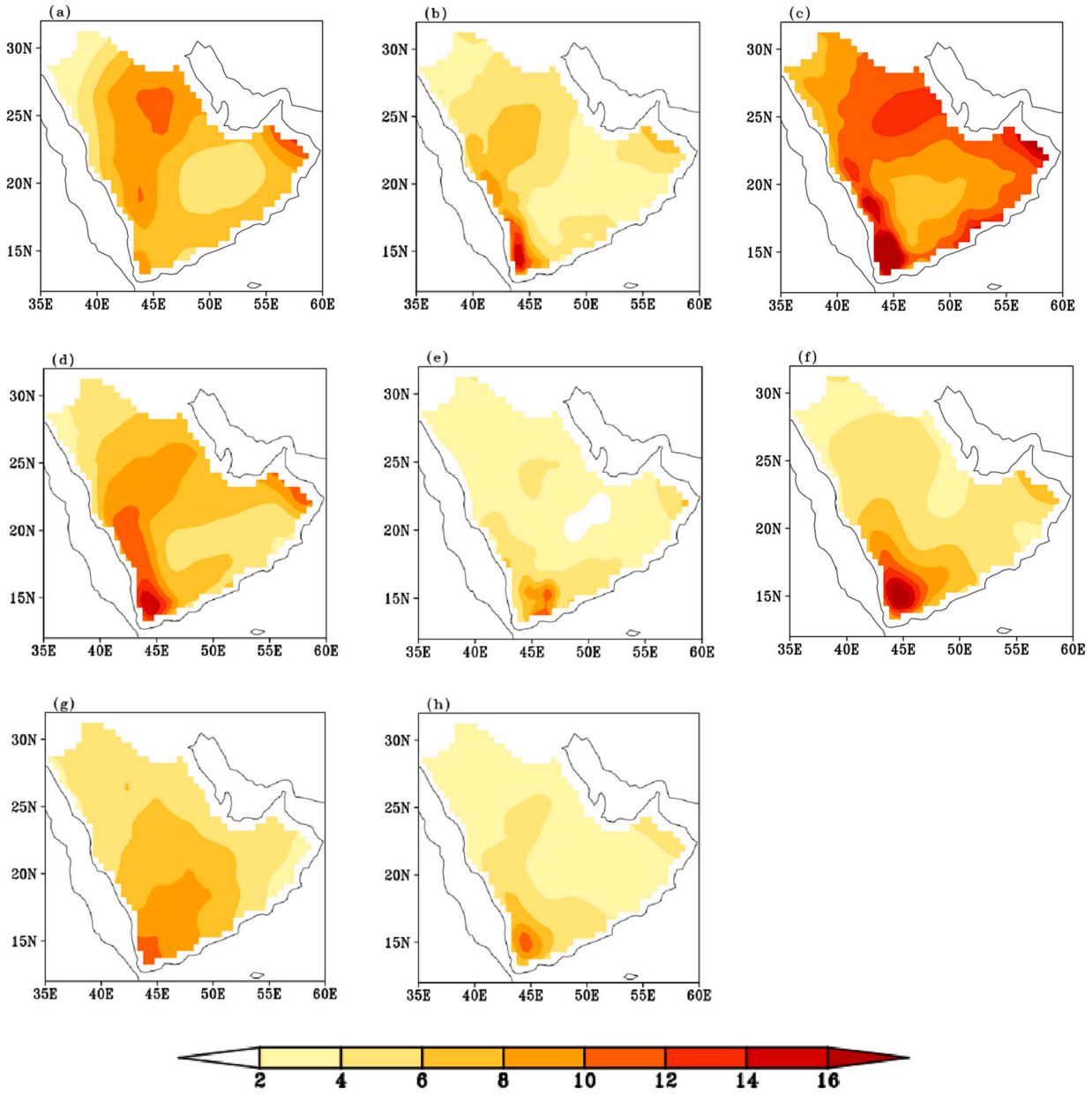

Fig. 4. Spring Season precipitation standard deviation from (a) GPCP, (b) SEAS, (c) METEOF, (d) UKMO, (e) DWD, (f) CMCC, (g) Saudi-KAU CGCMs, and (h) MME for the period 1993–2016.

prediction skill, while the curve bending toward the false-alarm rate axis reflects lower prediction skill (Kharin and Zwiers, 2003). The SEAS5 model shows low probability forecast skill for above and below normal conditions, and moderate level skill for normal events (Fig. 8a). The METEOF model shows low ROC scores and all three curves (above, normal, and below) are extended toward the false-alarm rate axis, indicating the poor skill of the model (Fig. 8b). However, the UKMO model displays high skill for above normal precipitation events, and satisfactory skill for normal and below normal situations (Fig. 8c). The DWD model demonstrates poor skill for all defined categories (Fig. 8d). The CMCC model attained low ROC scores for above and below normal events, but higher scores in the case of normal events (Fig. 8e). The Saudi-KAU model shows reasonably good skill for above and below normal conditions, but lower skill for normal precipitation events (Fig. 8f). Meanwhile, the MME shows low probabilistic forecast skill for above normal events (Fig. 8g). Overall, the Saudi-KAU and UKMO models show relatively higher skill compared to other models.

3.5. *Persistent prediction skill*

Fig. 9 shows a persistent prediction that provides a baseline to verify the prediction skill at various Lead Times (0–3). The skill is considered useful when it surpasses the persistent prediction. The seasonal persistent prediction is evaluated as lag k = 1 autocorrelation of observed precipitation index. The results shows that all models and MME depicts higher precipitation skill for Lead 0 and 1 while the lower skill is observed for Lead 3 over Arabian Peninsula. Moreover, all models and MME exhibits higher predictability for MAM, whereas the lower predictability is found in JAS. Further, the METEOF, UKMO, CMCC, and MME shows high skill while the Saudi-KAU and SEAS5 skill obtained in moderate range. In addition, the low skill is found in case of DWD model for most of the running seasons.

The signal variance of the C3S and Saudi-KAU models and the MME are displayed in Fig. S2. The METEOF, UKMO, CMCC, and Saudi-KAU models all have slightly high signal variance over almost all the

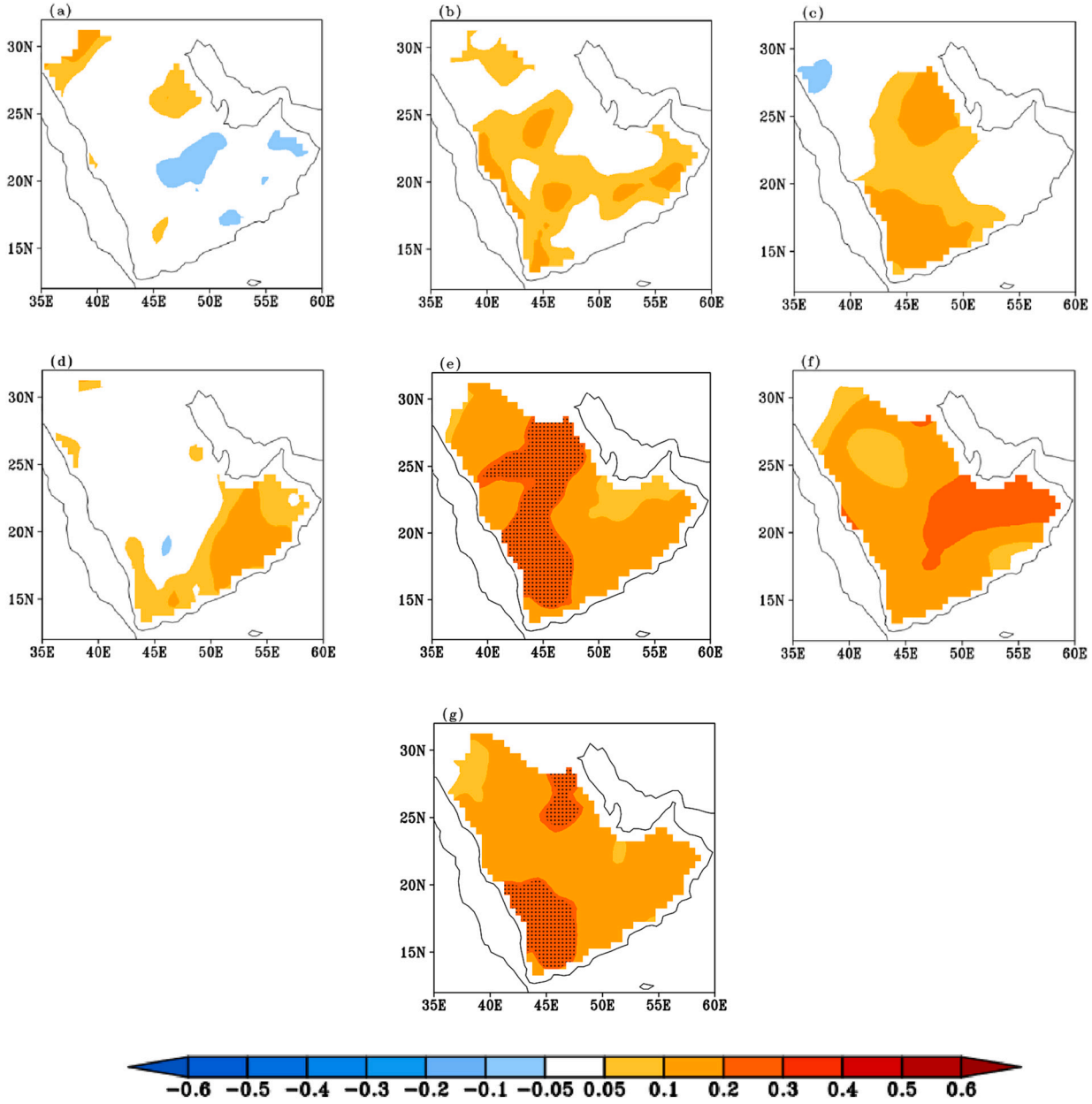

Fig. 5. Precipitation correlation skill during Spring season, from (a) SEAS, (b) METEOF, (c) UKMO, (d) DWD, (e) CMCC, (f) Saudi-KAU CGCM, (g) MME with respect to the GPCP observational data set. The significance (95 percentile) represents with stipples.

Peninsula, while the DWD, SEAS5, and MME show lower signal variance. Overall, the models all display almost identical spatial patterns of signal variance. High (low) signal variance is observed over southwestern, northeastern (northwestern, southeastern) regions of the Peninsula (Fig. S2a-g). Furthermore, the noise variance is presented in Fig. S3. The SEAS5 model shows high internal variability over the southwestern region, while low variability occurs over the northern and southeastern regions. METEOF displays high noise variance over almost all the Peninsula compared to the other models and the MME. The high (low) noise values are observed in southwestern (northwestern and southern) regions (Fig. S3b). The UKMO depicts high internal variance over southwestern regions but low variance over northern and southeastern regions (Fig. S3c). In addition, the DWD model shows low noise compared to other models over the entire Peninsula. The highest internal variability is seen over the southwestern region, while low noise is found over northwestern and southeastern regions (Fig. S3d). Furthermore, the CMCC and Saudi-KAU models and the MME display high noise variance over the southwestern region, and low variance over northern and southeastern regions (Fig. S3e-g).

3.6. *Predictability of individual models and multi-model ensemble mean*

Fig. 10 shows signal to noise ratio pattern of the individual Saudi-KAU and C3S models and the MME. SEAS5 and METEOF models attained low signal to noise ratios (0.05–0.1) compared to other models. Moreover, the UKMO, CMCC, and MME acquired reasonably good signal to noise ratios (0.1–0.25) over almost all the Peninsula while the DWD and Saudi-KAU models fall in a moderate range (0.05–0.15). All the models and the MME attained higher signal to noise ratios over the southwestern quadrant of the Peninsula, while lower values were obtained over the eastern and northern regions.

As mentioned in Section 2.3, the Rlimit value "0" means no predictability, while values approaching "1" reflect perfect predictability (Kang and Shukla, 2006; Westra and Sharma, 2010). The spatial

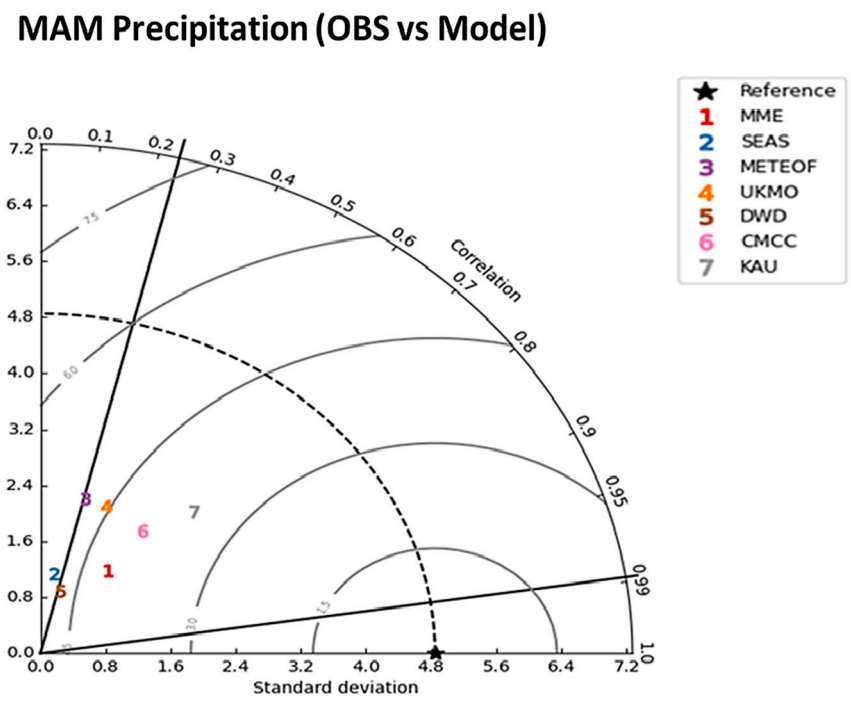

Fig. 6. Taylor diagram showing the performance of the MME and individual C3S and KAU models with respect to observations based on correlation co-efficient and standard deviations.

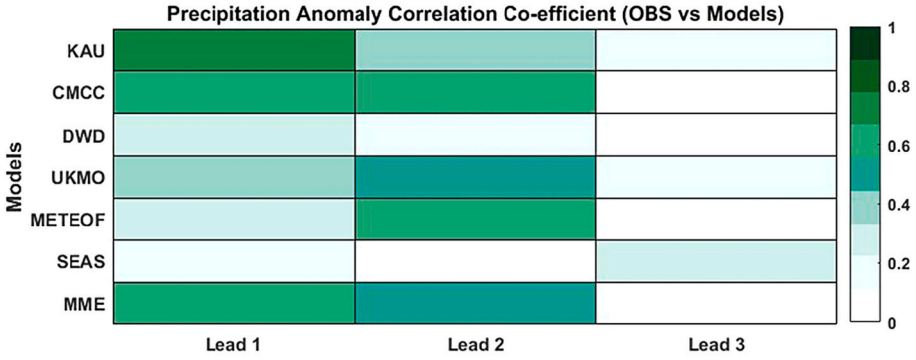

Fig. 7. Temporal Anomaly Correlation pattern of Arabian Peninsula precipitation for the spring season, from the MME, C3S models and Saudi-KAU CGCM with Lead Time (1–3).

distribution of the Rlimit patterns from the models and the MME are presented in Fig. 11. The UKMO, CMCC, and Saudi-KAU models all show relatively high predictability whereas the SEAS5 and DWD demonstrate low predictability. Almost all models report high Rlimit values over southwestern and northeastern regions, but comparatively lower values over northwestern and southeastern regions (Fig. 11a-g).

3.7. Observed and simulated teleconnection patterns

The spatial pattern of correlation between Arabian Peninsula springtime precipitation (AP-Prcp) and global SSTs are presented in Fig. 12. Several previous studies (Zheng et al., 2000; Phelps et al., 2004; Abid et al., 2018; Doi et al., 2020) considered a model to be reasonably good if it could reproduce the teleconnection patterns, since this also leads to high actual and potential predictability. Fig. 12a shows the correlation pattern between area-averaged observed Arabian Peninsula precipitation and global SSTs. The spring AP-Prcp has strong positive correlation with the equatorial Pacific and western Indian Ocean, whereas slightly negative correlations occur over the tropical Atlantic Ocean. These results show that Arabian Peninsula precipitation is modulated strongly by ENSO, as is affirmed by previous findings (e.g., Kang et al., 2015; Dasari et al., 2018). On the other hand, the SEAS5, METEOF, and UKMO models all weakly reproduced the teleconnection patterns (Fig. 12b-d). The DWD, CMCC, and Saudi-KAU models, and the MME, show a high positive correlation over the equatorial Indian and Pacific Oceans whereas these models and the MME display a low skill over the tropical Atlantic Ocean (Fig. 12e-h).

Fig. S4 shows the correlation pattern between Nino 3.4 and global SSTs, from observations, the C3S and Saudi-KAU models, and the MME for springtime. The observational pattern shows high correlation values over the tropical Indian and Pacific Oceans while a weak relationship is obtained over the tropical Atlantic Ocean. Almost all models are in line with observations and successfully capture the general pattern. However, the UKMO and Saudi-KAU models and the MME show a close correspondence, while the SEAS5 and DWD models depict slightly higher deviations compared to observations (Fig. S4a-h).

Correlations and Lead-Lag correlation matrix of observation, C3S, Saudi-KAU models and MME during the period 1993–2016 are shown in Table 2. The correlations of Arabian Peninsula spring precipitation and Nino3.4 SSTs shows that the significant correlation co-efficient value

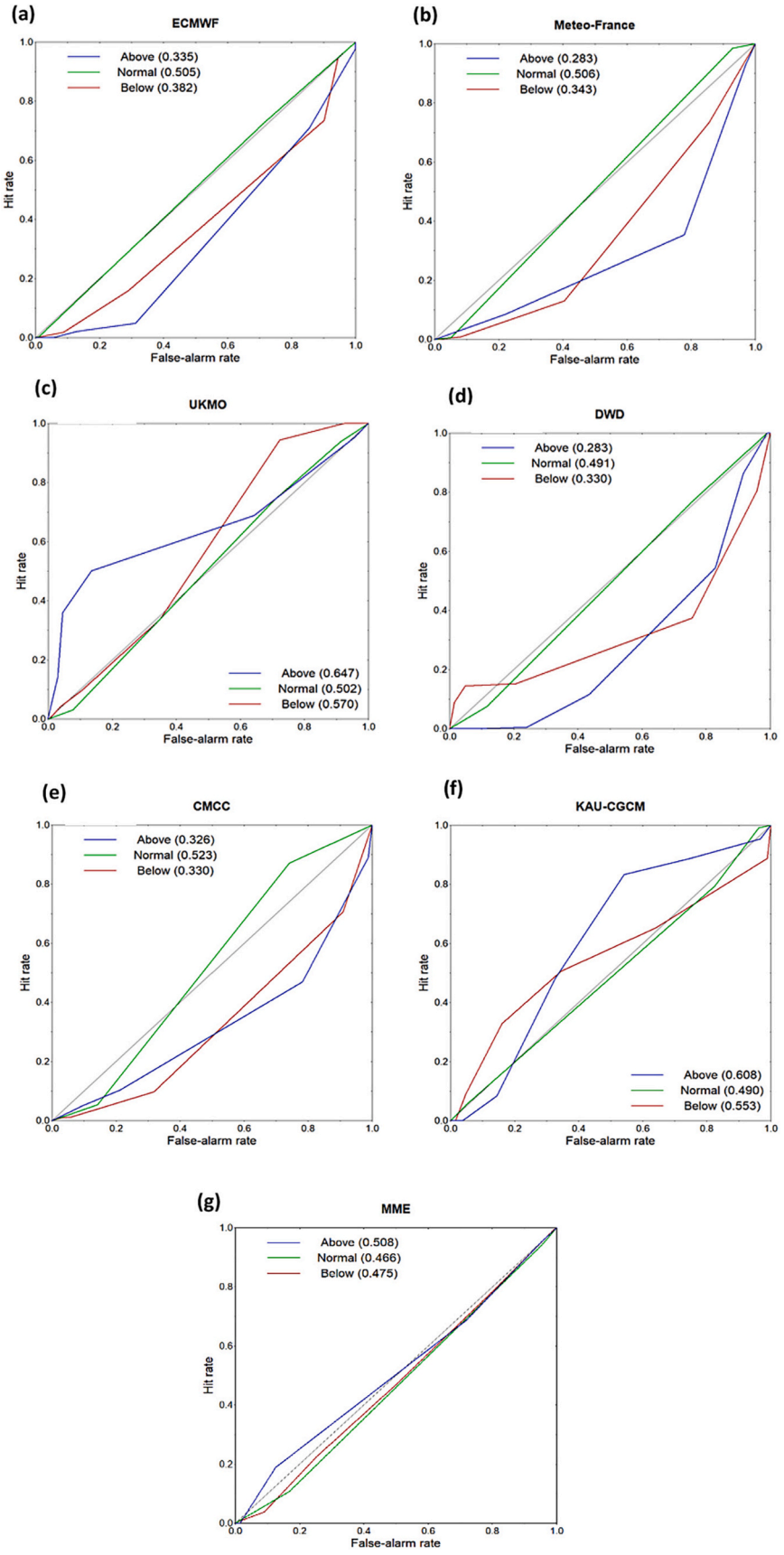

Fig. 8. Theoretical ROC curves for Probabilistic forecast of (a-e) C3S models, (f) Saudi-KAU GCM, and (g) MME, during the period 1993–2016.

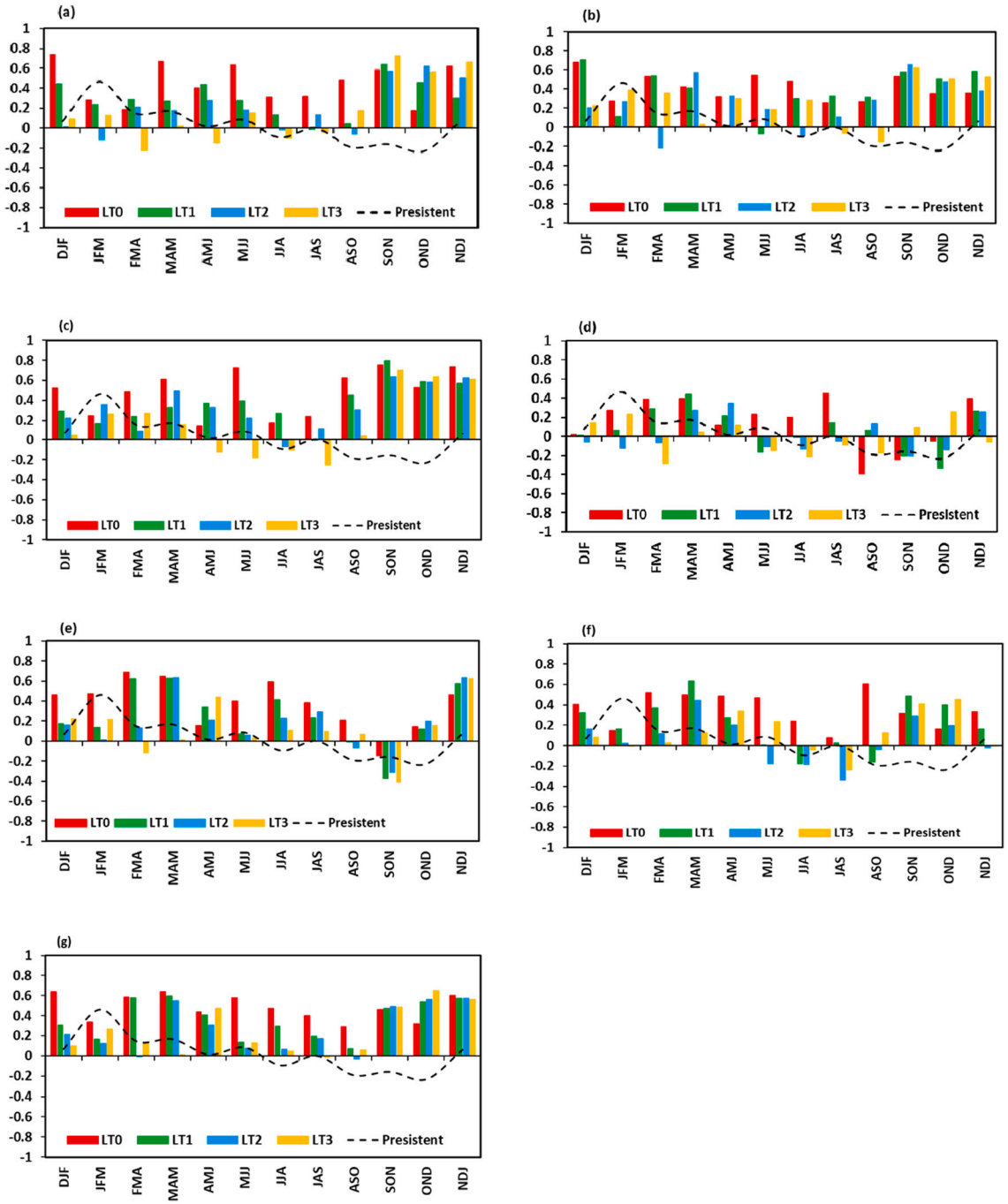

Fig. 9. Arabian Peninsula precipitation persistent skill of observations (black line) and prediction skill of models (a) SEAS5, (b) METEOF, (c) UKMO, (d) DWD, (e) CMCC, (f) Saudi-KAU models and (g) MME at different Lead Times (LT) 0 to 3 shown with color bars, LT0 (red), LT1 (green), LT2 (blue), and LT3 (yellow) during the running seasons. (For interpretation of the references to color in this figure legend, the reader is referred to the web version of this article.)

(0.51) obtained for observation, while the CMCC, DWD, Saudi-KAU, and MME presents relatively closer correlation values to observation. Moreover, the SEAS5 model shows low correlation co-efficient values for all Lead Times. In case of lead-lag correlation between winter ENSO SSTs (Nino3.4) and Arabian Peninsula spring precipitation a significant value obtained for observation (0.52), whereas the CMCC, DWD, and MME presents slightly high correlation co-efficient values. The METEOF and Saudi-KAU models acquired correlation co-efficient values in moderate range, while the low correlation co-efficient values found in case of SEAS5 and UKMO model. Ultimately, the results highlighted interesting fact that the spring Nino 3.4 and Arabian Peninsula precipitation shows high correlation values at Lead Time 3 (December Initial conditions) for most of the models. On the other hand, most of the models shows significant lead-lag correlation at Lead Time 1 which indicates that ENSO signal extended to spring and mainly responsible to modulate the Arabian Peninsula precipitation during spring.

3.8. Discussion

The present work focuses on the potential predictability and prediction skill of Saudi-KAU and C3S models for Arabian Peninsula spring precipitation. The analysis showed that all models and their MME demonstrate high potential predictability and skill over southwestern region which is crucial for Arabian Peninsula because this region is the

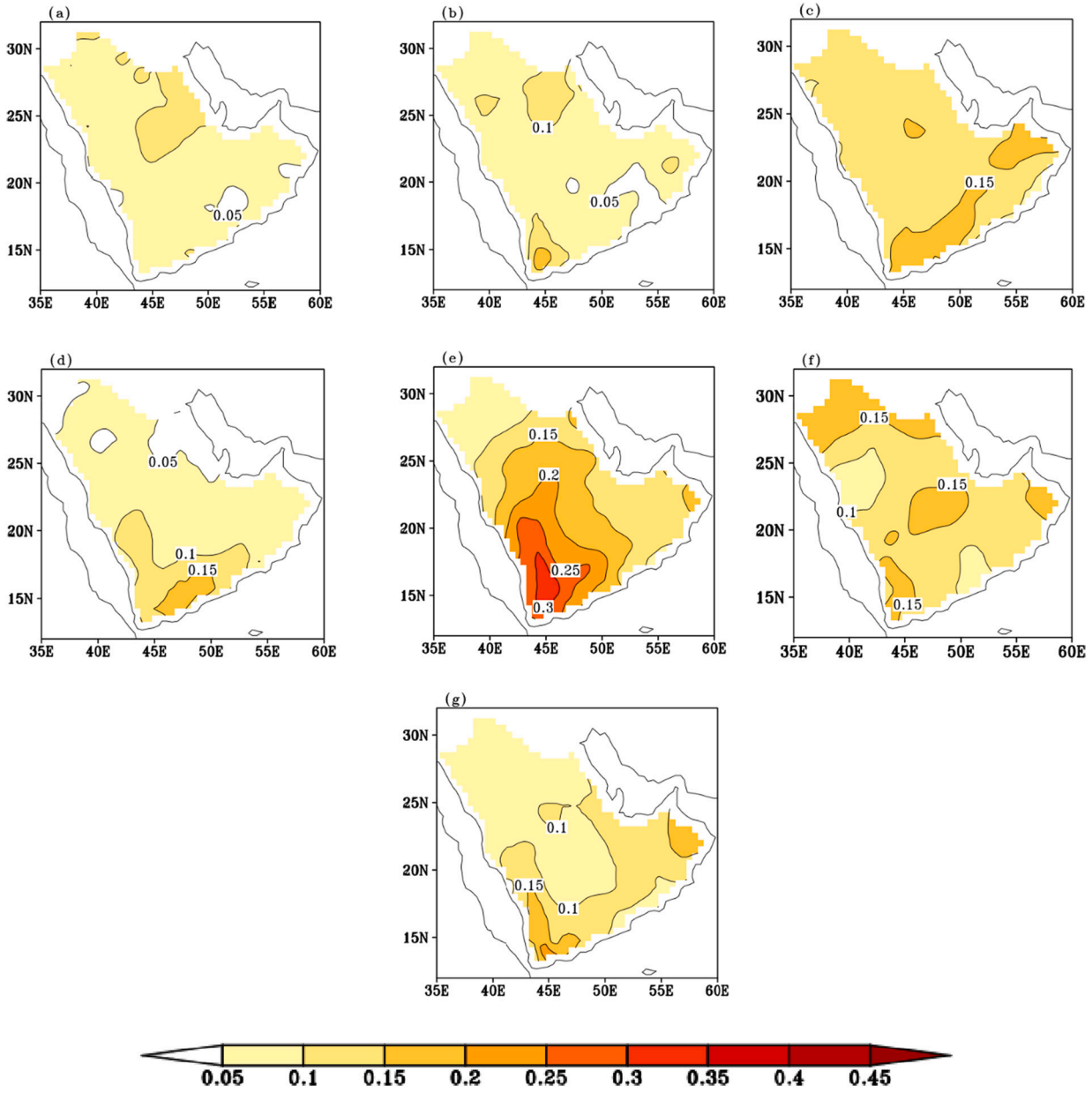

Fig. 10. Precipitation signal to noise ratio during the Spring season, from (a) SEAS, (b) METEOF, (c) UKMO, (d) DWD, (e) CMCC, (f) Saudi-KAU CGCM and (g) MME. The signal to noise ratio is computed for the period 1993 to 2016.

main contributor of total annual rainfall of Peninsula. This is in contrast with Abid et al. (2018) findings that showed high predictability and skill in southwestern domain. However, the predictability and prediction skill is obtained low at northern regions that may require further investigation to enhance the capability of models. Moreover, the displayed a strong linkage between Arabian Peninsula spring precipitation and ENSO. It is affirmed by various studies (i.e. Chandran et al., 2016; Niranjan Kumar et al., 2016; Sandeep and Ajayamohan, 2018) that ENSO dominantly influences the Arabian Peninsula precipitation. The positive phase of ENSO (El-Nino) brings more rainfall to the Peninsula while the negative phase (La-Nina) associated with drought conditions. It is also reported that the high (low) precipitation over Arabian Peninsula during El-Nino (La-Nina) is linked with the fluctuation of subtropical jet stream. On the other hand, the tropical North Atlantic Ocean also show a significant teleconnection pattern with the Arabian Peninsula spring precipitation. The north, south (central) Atlantic Ocean negative (positive) SSTs anomalies induces rainfall over Arabian Peninsula during spring. However, there are few studies available (e.g. Kumar et al., 2014; Hasanean and Almazroui, 2015; Donat et al., 2014) that discussed the negative phase of NAO causes more rainfall over Peninsula while the positive phase related with hot and dry conditions. In addition, the ROC analysis showed the probabilistic forecast skill of models for events with likelihood below normal, normal, and above normal. Overall, the CMCC, Saudi-KAU and UKMO models demonstrated high predictability and skill for Arabian Peninsula spring precipitation compared to other models. This study suggest that the model biases badly impact the potential predictability and prediction skill. The models uncertainties can be reduce by well defining the initial conditions, physics, and by increasing ensemble size.

Furthermore, in future may analyze the potential predictability and skill of climate models for Arabian Peninsula temperature.

4. Summary and conclusions

Seasonal prediction over any region is a valuable resource in order to enable stakeholders and decision makers to take timely preventative

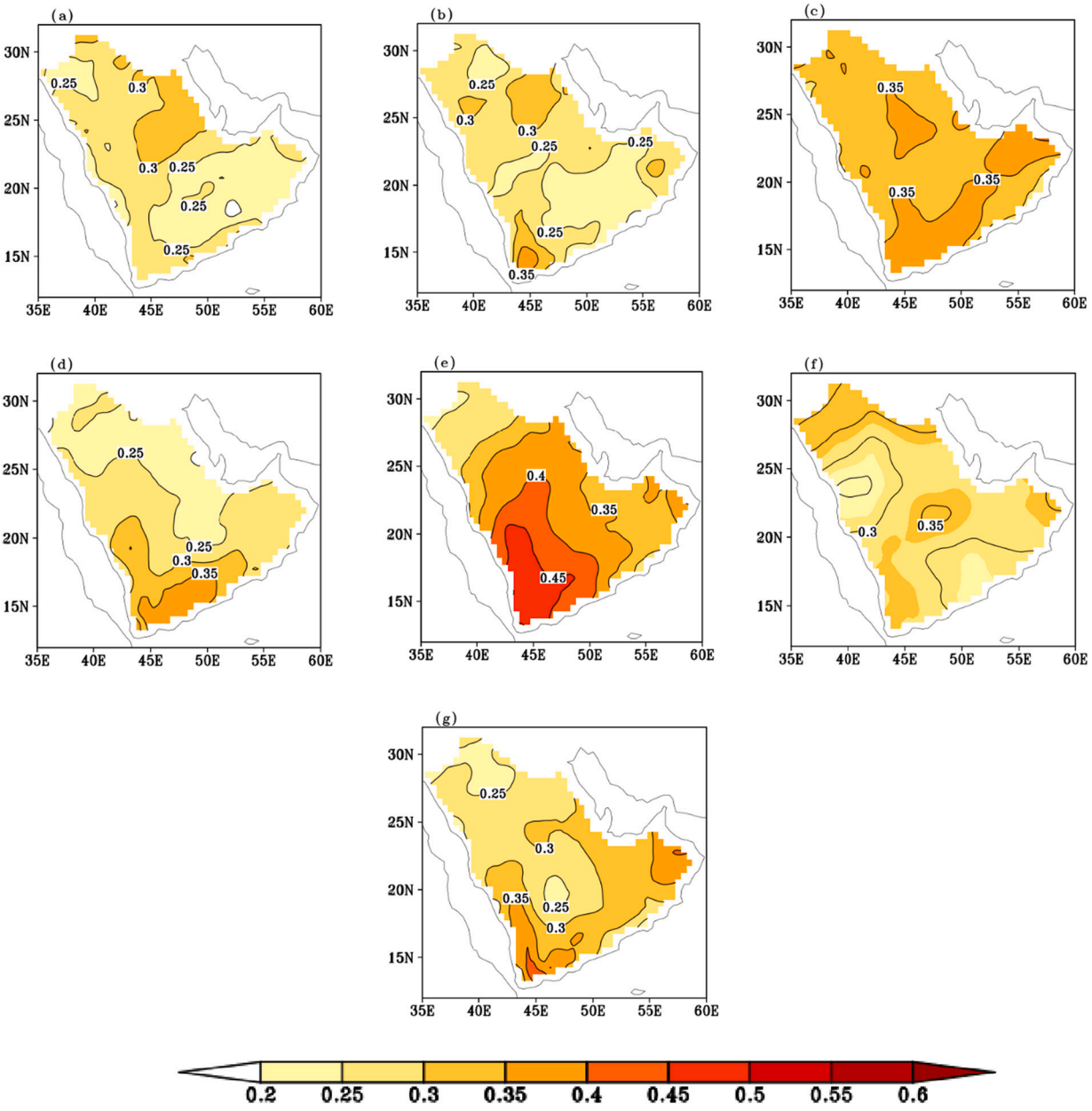

Fig. 11. Precipitation Rlimit during the Spring season, from (a) SEAS, (b) METEOF, (c) UKMO, (d) DWD, (e) CMCC, (f) Saudi-KAU CGCM, and (g) MME. The precipitation Rlimit is computed for the period 1993 to 2016.

actions. In the present study, we evaluated the potential predictability and prediction skill of spring precipitation over the Arabian Peninsula by using the simulated data of the Saudi-KAU and 5 C3S models for the period 1993–2016. The spring season has great importance in the Arabian Peninsula because 40% of the total annual rainfall comes from the spring season contribution (Alsaaran and Alghamdi, 2021). During spring, the southwestern regions of the Peninsula are affected more, due to convective rainfall that can cause flash flooding over the region (Samman and Gallus Jr, 2018). This provides strong motivation to assess the model's skill in simulating Arabian Peninsula spring precipitation. In the present work, the simulated data of 3-month lead time were examined, with Lead-1, Lead-2, and Lead-3 based on the Feb, Jan, and Dec initial conditions, respectively. We examined the individual model simulations as well as the multi-model ensemble (MME). The potential predictability of the individual models and the MME were assessed by the signal to noise ratio and theoretical limit of correlation skill, while the prediction skill was estimated by the temporal anomaly correlation co-efficient. Furthermore, the relative operating characteristic (ROC) analysis was performed to measure the probabilistic forecast skill. Our findings reveal that the CMCC, UKMO, and Saudi-KAU models show high S/N ratios (0.35, 0.22, and 0.21 respectively) over a widespread region of the Arabian Peninsula while the SEAS5 displays a low S/N ratio (< 0.15) over the entire Peninsula. Similarly, the theoretical limit of correlation skill results is in line with the S/N ratio outcomes. It is also noticed that all models and the MME show high (low) potential predictability over southwestern (northern) regions. The Saudi-KAU, CMCC, and MME all show a high correlation skill (0.68, 0.58, and 0.57 respectively) whereas the SEAS model shows low skill (0.14) for spring precipitation over the Peninsula. It is observed that prediction skill decreases with the increase of Lead time. Consequently, the ROC analysis revealed that the Saudi-KAU and UKMO models have relatively high probabilistic forecast skill compared to other models. Furthermore, all models and MME reasonably reproduce the Pacific (i.e. ENSO) teleconnection patterns, but demonstrate lower skill over tropical Atlantic

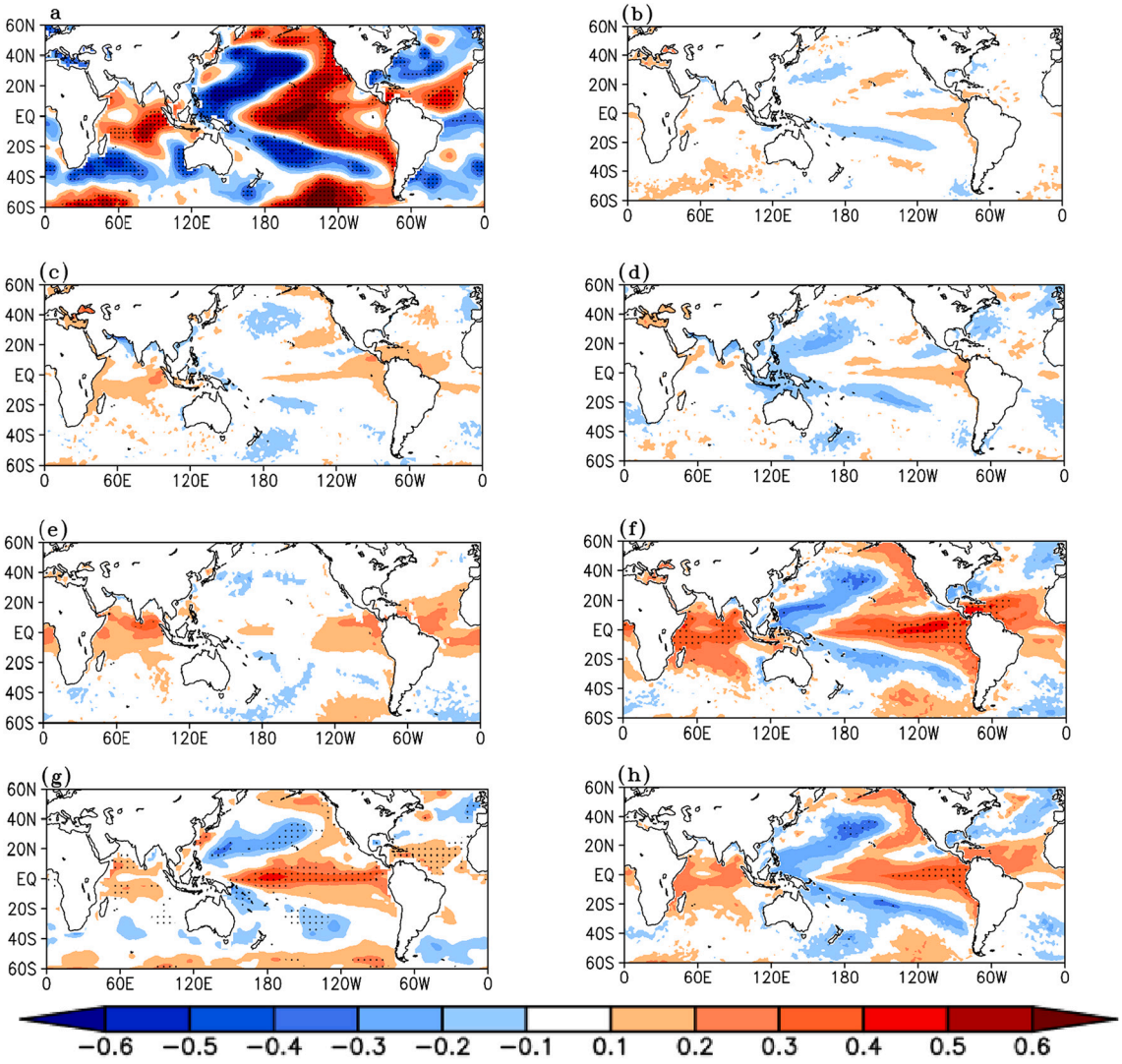

Fig. 12. Correlation pattern between spring precipitation over the Arabian Peninsula and (a) the Global SST observational data set, (b) SEAS, (c) METEOF, (d) UKMO, (e) DWD, (f) CMCC, (g) Saudi-KAU CGCM, and (h) MME for the period 1993 to 2016.The black stipples shows 95 percentile significance.

Table 2
Correlations and Lead-Lag correlation matrix of observation, C3S, Saudi-KAU models and MME during the period 1993–2016.

Correlations of Nino3.4-SSTs (MAM) and Arabian Peninsula Precipitation (MAM)								
	OBS	SEAS	METEOF	UKMO	DWD	CMCC	KAU	MME
	0.51	–	–	–	–	–	–	–
LT1	–	0.17	0.32	0.26	0.46	0.69	0.52	0.56
LT2	–	−0.24	0.36	0.17	0.49	0.91	0.60	0.63
LT3	–	0.28	0.67	0.60	0.63	0.82	0.48	0.68
Correlations of Nino3.4-SSTs (DJF) and Arabian Peninsula Precipitation (MAM)								
	OBS	SEAS	METEOF	UKMO	DWD	CMCC	KAU	MME
	0.52	–	–	–	–	–	–	–
LT1	–	−0.02	0.34	0.28	0.55	0.68	0.35	0.48
LT2	–	−0.35	0.22	0.17	0.55	0.76	0.29	0.45
LT3	–	0.10	0.58	−0.21	0.59	0.66	0.18	0.52

Ocean. Overall, the CMCC, Saudi-KAU and UKMO models show a relatively high potential predictability and prediction skill, whereas the SEAS5 model only poorly predicts spring precipitation over the Arabian Peninsula. The present work indicates that the model biases negatively impact the potential predictability and prediction skill. This can be overcome by improving initial conditions, model physics and by increasing the ensemble size. The present study provides insight into the potential and skill of the Saudi-KAU and C3S models for predicting Arabian Peninsula spring precipitation.

Authors statement

On behalf of all co-authors, I am the corresponding author stated that the manuscript is original and all authors contributed in its analysis, preparation and revision.

Two co-authors Muhammad Azhar Ehsan from International Research Institute for Climate and Society, Columbia Climate School, Columbia University, Palisades, NY, USA and Muhammad Adnan Abid from The Abdus Salam International Center for Theoretical Physics, Trieste, Italy are added because of their substantial contribution during the revision.

Declaration of Competing Interest

The authors declare the following financial interests/personal relationships which may be considered as potential competing interests.

The authors declare that there is no conflict of interest.

Data availability

The authors do not have permission to share data.

Acknowledgments

The authors thank the Center of Excellence for Climate Change Research for archiving and providing free access to the Saudi-KAU dataset. The C3S and GPCC datasets were obtained from their websites. The computation work and data analysis were performed on the Aziz Supercomputer at King Abdulaziz University's High–Performance Computing Center, Jeddah, Saudi Arabia.

Appendix A. Supplementary data

Supplementary data to this article can be found online at https://doi.org/10.1016/j.atmosres.2022.106461.

References

Abid, M.A., Kucharski, F., Almazroui, M., Kang, I., 2016. Interannual rainfall variability and ECMWF-Sys4-based predictability over the Arabian Peninsula winter monsoon region. Q. J. R. Meteorol. Soc. 142, 233–242.

Abid, M.A., Almazroui, M., Kucharski, F., O'Brien, E., Yousef, A.E., 2018. ENSO relationship to summer rainfall variability and its potential predictability over Arabian Peninsula region. NPJ Clim. Atmos. Sci. 1, 1–7.

Adler, R.F., Huffman, G.J., Chang, A., Ferraro, R., Xie, P.-P., Janowiak, J., Rudolf, B., Schneider, U., Curtis, S., Bolvin, D., 2003. The version-2 global precipitation climatology project (GPCP) monthly precipitation analysis (1979–present). J. Hydrometeorol. 4, 1147–1167.

Alamgir, M., Mohsenipour, M., Homsi, R., Wang, X., Shahid, S., Shiru, M.S., Alias, N.E., Yuzir, A., 2019. Parametric assessment of seasonal drought risk to crop production in Bangladesh. Sustainability 11, 1442.

Almazroui, M., 2013. Simulation of present and future climate of Saudi Arabia using a regional climate model (PRECIS). Int. J. Climatol. 33, 2247–2259.

Almazroui, M., 2020. Changes in temperature trends and extremes over Saudi Arabia for the period 1978–2019. Adv. Meteorol. 2020.

Almazroui, M., Saeed, S., 2020. Contribution of extreme daily precipitation to total rainfall over the Arabian Peninsula. Atmos. Res. 231, 104672.

Almazroui, M., Nazrul Islam, M., Athar, H., Jones, P.D., Rahman, M.A., 2012. Recent climate change in the Arabian Peninsula: annual rainfall and temperature analysis of Saudi Arabia for 1978–2009. Int. J. Climatol. 32, 953–966.

Almazroui, M., Tayeb, O., Mashat, A.S., Yousef, A., Al-Turki, Y.A., Abid, M.A., Bafail, A. O., Ehsan, M.A., Zahed, A., Rahman, M.A., 2017. Saudi-KAU coupled global climate model: description and performance. Earth Syst. Environ. 1, 1–23.

Almazroui, M., Khalid, M.S., Islam, M.N., Saeed, S., 2020. Seasonal and regional changes in temperature projections over the Arabian Peninsula based on the CMIP5 multi-model ensemble dataset. Atmos. Res. 239 https://doi.org/10.1016/j.atmosres.2020.104913.

Almazroui, M., Ehsan, M.A., Tippett, M.K., Ismail, M., Islam, M.N., Camargo, S.J., Abid, M.A., O'Brien, E., Kamil, S., Robertson, A.W., 2022. Skill of the Saudi-KAU CGCM in forecasting ENSO and its Comparison with NMME and C3S Models. Earth Syst. Environ. 1–15.

Alsaaran, N.A., Alghamdi, A.S., 2021. Precipitation climatology and spatiotemporal trends over the Arabian Peninsula. Theor. Appl. Climatol. 1–17.

AlSarmi, S.H., Washington, R., 2014. Changes in climate extremes in the Arabian Peninsula: analysis of daily data. Int. J. Climatol. 34, 1329–1345.

Attada, R., Dasari, H.P., Chowdary, J.S., Yadav, R.K., Knio, O., Hoteit, I., 2019. Surface air temperature variability over the Arabian Peninsula and its links to circulation patterns. Int. J. Climatol. 39, 445–464.

Bahaga, T.K., Mengistu Tsidu, G., Kucharski, F., Diro, G.T., 2015. Potential predictability of the sea-surface temperature forced equatorial East African short rains interannual variability in the 20th century. Q. J. R. Meteorol. Soc. 141, 16–26.

Barfus, K., Bernhofer, C., 2014. Assessment of GCM performances for the Arabian Peninsula, Brazil, and Ukraine and indications of regional climate change. Environ. Earth Sci. 72, 4689–4703.

Barnston, A.G., Tippett, M.K., L'Heureux, M.L., Li, S., DeWitt, D.G., 2012. Skill of real-time seasonal ENSO model predictions during 2002–11: is our capability increasing? Bull. Am. Meteorol. Soc. 93, 631–651.

Barnston, A.G., Tippett, M.K., Ranganathan, M., L'Heureux, M.L., 2019. Deterministic skill of ENSO predictions from the north American Multimodel Ensemble. Clim. Dyn. 53, 7215–7234.

Becker, E., den Dool, H., van Zhang, Q., 2014. Predictability and forecast skill in NMME. J. Clim. 27, 5891–5906.

Bett, P.E., Thornton, H.E., Troccoli, A., De Felice, M., Suckling, E., Dubus, L., Saint-Drenan, Y.-M., Brayshaw, D.J., 2019. A Simplified Seasonal Forecasting Strategy, Applied to Wind and Solar Power in Europe.

Bourke, W., 1974. A multi-level spectral model. I. Formulation and hemispheric integrations. Mon. Weather Rev. 102, 687–701.

Bucchignani, E., Mercogliano, P., Panitz, H.-J., Montesarchio, M., 2018. Climate change projections for the Middle East–North Africa domain with COSMO-CLM at different spatial resolutions. Adv. Clim. Chang. Res. 9, 66–80.

Cash, B.A., Manganello, J.V., Kinter, J.L., 2019. Evaluation of NMME temperature and precipitation bias and forecast skill for South Asia. Clim. Dyn. 53, 7363–7380.

Chandran, A., Basha, G., Ouarda, T., 2016. Influence of climate oscillations on temperature and precipitation over the United Arab Emirates. Int. J. Climatol. 36, 225–235.

Chaturvedi, S., Cheong, T.S., Luo, Y., Singh, C., Shaw, R., 2022. IPCC Sixth Assessment Report (AR6): Climate Change 2022-Impacts, Adaptation and Vulnerability: Regional Factsheet Asia.

Cheng, Y., Tang, Y., Chen, D., 2011. Relationship between predictability and forecast skill of ENSO on various time scales. J. Geophys. Res. Ocean 116.

Contreras, E., Herrero, J., Crochemore, L., Aguilar, C., Polo, M.J., 2020. Seasonal climate forecast skill assessment for the management of water resources in a run of river hydropower system in the Poqueira River (Southern Spain). Water 12, 2119.

Dasari, H.P., Langodan, S., Viswanadhapalli, Y., Vadlamudi, B.R., Papadopoulos, V.P., Hoteit, I., 2018. ENSO influence on the interannual variability of the Red Sea convergence zone and associated rainfall. Int. J. Climatol. 38, 761–775.

Doi, T., Nonaka, M., Behera, S., 2020. Skill assessment of seasonal-to-interannual prediction of sea level anomaly in the north pacific based on the SINTEX-F climate model. Front. Mar. Sci. 7, 546587.

Donat, M.G., Peterson, T.C., Brunet, M., King, A.D., Almazroui, M., Kolli, R.K., Boucherf, D., Al-Mulla, A.Y., Nour, A.Y., Aly, A.A., 2014. Changes in extreme temperature and precipitation in the Arab region: long-term trends and variability related to ENSO and NAO. Int. J. Climatol. 34, 581–592.

Ehsan, M.A., Almazroui, M., Yousef, A., Tippett, M.K., Kucharski, F., Alkhalaf, A.A., 2017. Sensitivity of AGCM-simulated regional JJAS precipitation to different convective parameterization schemes. Int. J. Climatol. 37, 4594–4609.

Ehsan, M.A., Kucharski, F., Almazroui, M., Ismail, M., Tippett, M.K., 2019. Potential predictability of Arabian Peninsula summer surface air temperature in the North American multimodel ensemble. Clim. Dyn. 53, 4249–4266.

Fröhlich, K., Dobrynin, M., Isensee, K., Gessner, C., Paxian, A., Pohlmann, H., Haak, H., Brune, S., Früh, B., Baehr, J., 2021. The German climate forecast system: GCFS. J. Adv. Model. Earth Syst. 13, e2020MS002101.

Gebrechorkos, S.H., Pan, M., Beck, H.E., Sheffield, J., 2022. Performance of State-of-the-Art C3S European seasonal climate forecast models for mean and extreme precipitation over Africa. Water Resour. Res. 58, e2021WR031480.

Giuntoli, I., Fabiano, F., Corti, S., 2021. Seasonal predictability of Mediterranean weather regimes in the Copernicus C3S systems. Clim. Dyn. 1–17.

Giuntoli, I., Fabiano, F., Corti, S., 2022. Seasonal predictability of Mediterranean weather regimes in the Copernicus C3S systems. Clim. Dyn. 58, 2131–2147.

Guérémy, J.-F., Dubois, C., Viel, C., Dorel, L., Ardilouze, C., Batte, L., Richon, J., Xu, Y., Nicolay, F., Soubeyroux, J.-M., 2021. Assessment of Météo-France current seasonal forecasting system S7 and outlook on the upcoming S8. In: EGU General Assembly Conference Abstracts. EGU21-10185.

Hasanean, H., Almazroui, M., 2015. Rainfall: features and variations over Saudi Arabia, a review. Climate 3, 578–626.

Hoffman, R.N., Kalnay, E., 1983. Lagged average forecasting, an alternative to Monte Carlo forecasting. Tellus A Dyn. Meteorol. Oceanogr. 35, 100–118.

Huang, B., Thorne, P.W., Banzon, V.F., Boyer, T., Chepurin, G., Lawrimore, J.H., Menne, M.J., Smith, T.M., Vose, R.S., Zhang, H.-M., 2017. Extended reconstructed sea surface temperature, version 5 (ERSSTv5): upgrades, validations, and intercomparisons. J. Clim. 30, 8179–8205.

IPCC, 2022. Climate Change 2022: Mitigation of Climate Change. Contribution of Working Group III to the Sixth Assessment Report of the Intergovernmental Panel on Climate Change. Cambridge University Press, Cambridge, UK and New York, NY, USA.

Jia, L., Yang, X., Vecchi, G.A., Gudgel, R.G., Delworth, T.L., Rosati, A., Stern, W.F., Wittenberg, A.T., Krishnamurthy, L., Zhang, S., 2015. Improved seasonal prediction of temperature and precipitation over land in a high-resolution GFDL climate model. J. Clim. 28, 2044–2062.

Jin, Y., Rong, X., Liu, Z., 2018. Potential predictability and forecast skill in ensemble climate forecast: a skill-persistence rule. Clim. Dyn. 51, 2725–2742.
Johnson, S., Stockdale, T., Ferranti, L., Molteni, F., Balmaseda, M.A., Weisheimer, A., Vitart, F., 2019. A study of teleconnections in state-of-the-art seasonal forecast systems. AGU Fall Meeting Abstracts. A21H–2724.
Kang, I.-S., Shukla, J., 2006. Dynamic seasonal prediction and predictability of the monsoon. In: The Asian Monsoon. Springer, pp. 585–612.
Kamil, S., Almazroui, M., Kucharski, F., Kang, I.S., 2017. Multidecadal changes in the relationship of storm frequency over euro-mediterranean region and ENSO during boreal winter. Earth Syst. Environ. 1 (1), 1–10.
Kang, I.-S., Rashid, I.U., Kucharski, F., Almazroui, M., Alkhalaf, A.K., 2015. Multidecadal changes in the relationship between ENSO and wet-season precipitation in the Arabian Peninsula. J. Clim. 28, 4743–4752.
Khan, M.Z.K., Sharma, A., Mehrotra, R., 2017. Global seasonal precipitation forecasts using improved sea surface temperature predictions. J. Geophys. Res. Atmos. 122, 4773–4785.
Kharin, V.V., Zwiers, F.W., 2003. On the ROC score of probability forecasts. J. Clim. 16, 4145–4150.
Kotwicki, V., Al Sulaimani, Z., 2009. Climates of the Arabian Peninsula–past, present, future. Int. J. Clim. Chang. Strateg. Manag.
Krakauer, N.Y., 2019. Temperature trends and prediction skill in NMME seasonal forecasts. Clim. Dyn. 53, 7201–7213.
Kumar, Ni, Abouelmagd, A.A., McCabe, M.F., Molini, A., 2014. Precipitation over the Arabian Peninsula: Global Forcing and Tele-connections. In: EGU General Assembly Conference Abstracts, p. 11545.
MacLachlan, C., Arribas, A., Peterson, K.A., Maidens, A., Fereday, D., Scaife, A.A., Gordon, M., Vellinga, M., Williams, A., Comer, R.E., 2015. Global seasonal forecast system version 5 (GloSea5): a high-resolution seasonal forecast system. Q. J. R. Meteorol. Soc. 141, 1072–1084.
Manzanas, R., Amekudzi, L.K., Preko, K., Herrera, S., Gutiérrez, J.M., 2014. Precipitation variability and trends in Ghana: an intercomparison of observational and reanalysis products. Clim. Chang. 124, 805–819. https://doi.org/10.1007/s10584-014-1100-9.
Min, Y.-M., Ham, S., Yoo, J.-H., Han, S.-H., 2020. Recent progress and future prospects of subseasonal and seasonal climate predictions. Bull. Am. Meteorol. Soc. 101, E640–E644.
Nelli, N.R., Francis, D., Fonseca, R., Abida, R., Weston, M., Wehbe, Y., Al Hosary, T., 2021. The atmospheric controls of extreme convective events over the southern Arabian Peninsula during the spring season. Atmos. Res. 262, 105788.
Niranjan Kumar, K., Ouarda, T.B.M.J., Sandeep, S., Ajayamohan, R.S., 2016. Wintertime precipitation variability over the Arabian Peninsula and its relationship with ENSO in the CAM4 simulations. Clim. Dyn. 47, 2443–2454.
Nobakht, M., Saghafian, B., Aminyavari, S., 2021. Skill assessment of Copernicus climate change Service seasonal ensemble precipitation forecasts over Iran. Adv. Atmos. Sci. 38, 504–521.
Odnoletkova, N., Patzek, T.W., 2021. Data-driven analysis of climate change in Saudi Arabia: trends in temperature extremes and human comfort indicators. J. Appl. Meteorol. Climatol. 60, 1055–1070.
Osman, M., Vera, C.S., 2017. Climate predictability and prediction skill on seasonal time scales over South America from CHFP models. Clim. Dyn. 49, 2365–2383.
Pal, J.S., Eltahir, E.A.B., 2016. Future temperature in Southwest Asia projected to exceed a threshold for human adaptability. Nat. Clim. Chang. 6, 197–200.
Patlakas, P., Stathopoulos, C., Flocas, H., Bartsotas, N.S., Kallos, G., 2021. Precipitation climatology for the arid region of the Arabian Peninsula—variability, trends and extremes. Climate 9, 103.
Phelps, M.W., Kumar, A., O'Brien, J.J., 2004. Potential predictability in the NCEP CPC dynamical seasonal forecast system. J. Clim. 17, 3775–3785.
Pincus, R., Batstone, C.P., Hofmann, R.J.P., Taylor, K.E., Glecker, P.J., 2008. Evaluating the present-day simulation of clouds, precipitation, and radiation in climate models. J. Geophys. Res. Atmos. 113.
Rahman, M.A., Almazroui, M., Islam, M.N., O'Brien, E., Yousef, A.E., 2018. The role of land surface fluxes in Saudi-KAU AGCM: temperature climatology over the Arabian Peninsula for the period 1981–2010. Atmos. Res. 200, 139–152.
Rana, S., Renwick, J., McGregor, J., Singh, A., 2018. Seasonal prediction of winter precipitation anomalies over Central Southwest Asia: a canonical correlation analysis approach. J. Clim. 31, 727–741.
Rashid, I.U., Abid, M.A., Almazroui, M., Kucharski, F., Hanif, M., Ali, S., Ismail, M., 2022. Early summer surface air temperature variability over Pakistan and the role of El Niño–Southern Oscillation teleconnections. Int. J. Climatol. 42 (11), 5768–5784. https://doi.org/10.1002/joc.7560.
Risbey, J.S., Squire, D.T., Black, A.S., DelSole, T., Lepore, C., Matear, R.J., Monselesan, D. P., Moore, T.S., Richardson, D., Schepen, A., 2021. Standard assessments of climate forecast skill can be misleading. Nat. Commun. 12, 1–14.
Rowell, D.P., 1998. Assessing potential seasonal predictability with an ensemble of multidecadal GCM simulations. J. Clim. 11, 109–120.
Rowell, D.P., Folland, C.K., Maskell, K., Ward, M.N., 1995. Variability of summer rainfall over tropical North Africa (1906–92): Observations and modelling. Q. J. R. Meteorol. Soc. 121, 669–704.
Samman, A.E., Gallus Jr., W.A., 2018. A classification of synoptic patterns inducing heavy precipitation in Saudi Arabia during the period 2000-2014. Atmósfera 31, 47–67.
Sandeep, S., Ajayamohan, R.S., 2018. Modulation of winter precipitation dynamics over the Arabian Gulf by ENSO. J. Geophys. Res. Atmos. 123, 198–210.
Sanna, A., Borelli, A., Athanasiadis, P., Materia, S., Storto, A., Navarra, A., Tibaldi, S., Gualdi, S., 2017. RP0285—CMCC-SPS3: the CMCC seasonal prediction system 3. CMCC Tech. Rep. RP0285, p.61. https://www.cmcc.it/it/publications/rp0285-cmcc-sps3-the-cmcc-seasonal-prediction-system-3/.
Syed, F.S., Latif, M., Al-Maashi, A., Ghulam, A., 2019. Regional climate model RCA4 simulations of temperature and precipitation over the Arabian Peninsula: sensitivity to CORDEX domain and lateral boundary conditions. Clim. Dyn. 53, 7045–7064.
Taylor, K.E., 2001. Summarizing multiple aspects of model performance in a single diagram. J. Geophys. Res. 106, 7183–7192.
Tebaldi, C., Knutti, R., 2007. The use of the multi-model ensemble in probabilistic climate projections. Philos. Trans. R. Soc. A Math. Phys. Eng. Sci. 365, 2053–2075.
Vitart, F., Robertson, A.W., 2018. The sub-seasonal to seasonal prediction project (S2S) and the prediction of extreme events. NPJ Clim. Atmos. Sci. 1, 1–7.
Vitart, F., Ardilouze, C., Bonet, A., Brookshaw, A., Chen, M., Codorean, C., Déqué, M., Ferranti, L., Fucile, E., Fuentes, M., 2017. The subseasonal to seasonal (S2S) prediction project database. Bull. Am. Meteorol. Soc. 98, 163–173.
Wang, B., Lee, J.-Y., Xiang, B., 2015. Asian summer monsoon rainfall predictability: a predictable mode analysis. Clim. Dyn. 44, 61–74.
Watson, R.T., Albritton, D.L., Dokken, D.J., 2001. Climate Change 2001: Synthesis Report. Cambridge University Press Cambridge, UK.
Wei, T., Zhao-Hui, L., Li-Feng, L., 2013. Assessing the seasonal predictability of summer precipitation over the Huaihe River basin with multiple APCC models. Atmos. Ocean. Sci. Lett. 6, 185–190.
Weisheimer, A., Palmer, T.N., 2014. On the reliability of seasonal climate forecasts. J. R. Soc. Interface 11, 20131162.
Westra, S., Sharma, A., 2010. An upper limit to seasonal rainfall predictability? J. Clim. 23, 3332–3351.
Zheng, X., Nakamura, H., Renwick, J.A., 2000. Potential predictability of seasonal means based on monthly time series of meteorological variables. J. Clim. 13, 2591–2604.
Zuo, J., Ren, H.-L., Wu, J., Nie, Y., Li, Q., 2016. Subseasonal variability and predictability of the Arctic Oscillation/North Atlantic Oscillation in BCC_AGCM2. 2. Dyn. Atmos. Ocean. 75, 33–45.